Obtaining 1D Dynamics in a Quasi-1D NMR Spin System

by

Brian Jeffrey Pepper

Submitted to the Department of Physics
in partial fulfillment of the requirements for the degree of

BACHELOR OF SCIENCE

at the

MASSACHUSETTS INSTITUTE OF TECHNOLOGY

June 2008

Author .....
Department of Physics
May 20, 2008

Certified by .....
David G. Cory
Professor of Nuclear Science and Engineering
Thesis Supervisor

Accepted by .....
David E. Pritchard
Senior Thesis Coordinator, Department of Physics

Obtaining 1D Dynamics in a Quasi-1D NMR Spin System

by

Brian Jeffrey Pepper

Submitted to the Department of Physics
on May 20, 2008, in partial fulfillment of the
requirements for the degree of
BACHELOR OF SCIENCE

Abstract

In this thesis, I explored the evolution and dynamics of multiple quantum coherences in a quasi-1D crystal lattice, Fluorapatite (FAp), through the use of NMR. In particular I focused on the system with chains aligned with the magnetic field axis, and with the so-called "magic angle" of 54.7°. In addition, I created a new method of rotation and long RF pulses for NMR spectroscopy. The method cancels off-chain terms of the dipolar Hamiltonian in quasi-1D lattices, while preserving on-chain terms. This allows 1D dynamics to dominate for longer timescales. Finally, a framework is proposed by which one could generalize this method to other systems; similarly cancelling some set of "undesirable" dipolar couplings while preserving others. This method has applications in Quantum Information Processing (QIP), where it could lead to the experimental realization of a 1D spin chain, a system that has provoked much theoretical interest, and the framework has larger implications for simulation of other quantum systems.

Thesis Supervisor: David G. Cory
Title: Professor of Nuclear Science and Engineering

Acknowledgments

First, I would like to thank to David Cory for all his help and advice. His recommendations on the direction with which to approach problems have been particularly helpful throughout my time at his lab. I would also like to thank him for his guidance in the writing of this thesis.

I am grateful to Sekhar Ramanathan. His explanations of complex topics were amazingly clear, and his door was always open. I am particularly grateful for his advice concerning careers.

I am grateful to those I worked with in this lab, particularly: Paola Cappellaro, whose work essentially created my own; Peter Allen, who helped me construct a new probe head; Natania Antler, who provided scripts and a pulse sequence used in my work; and Kai Iamsumang, who helped keep my experiments running.

I would like to thank all of my professors. Their instruction has made me a better physicist, but it has done more than that; it has forced me to adapt, and learn how to approach hard problems. I would like to thank a few in particular: Max Tegmark, whose lectures made me fall in love with physics; Julian Wheatley, whose one rule ("No mistakes.") I will try to live by; and Isaac Chuang, who pushed me harder and demanded more.

I would like to thank my family. Their unconditional love and support has made me the person I am today. They have always been there for me, and it is only with their help that I have made it to where I am today.

Finally, I would like to thank my friends, they were there for me and kept me going. Sometimes we place too little value on our own sanity, on stopping to enjoy the experiences. Four years went by in an instant, so thank you, Libby, Dennis, Liz, Alex, Irene, Nick, and others, for reminding me to open doors I haven't seen before.

Contents

List of Figures

Chapter 1

Introduction

NMR is a useful tool that has been applied to study quantum information processing. Since Lloyd's proposal of using liquid-state NMR as a testbed, and its subsequent exprimental realization [9], NMR has been an excellent way to test quantum algorithms at the small scale.

However, these liquid-state systems are not scaleable [4, 6, 5], due to the complexity of the coupling network of such molecules. Thus, there is interest in solid-state NMR using only one type of atom, either for transmission of quantum states or for mapping to a more complex quantum system. Solid state NMR holds promise both for quantum information processing and for simulation of complex quantum spin systems, such as might be seen in condensed matter theory.

The challenge with using a solid-state system lies in addressing individual spins; how are we to manipulate one spin if all spins resonate at the same frequency? Results show, however, that in a 1D spin system, all that is needed to achieve universal control are pulses which manipulate the whole chain and pulses which manipulate the spins at the ends of the chain [15]. For this reason, researchers have taken particular interest in 1D spin systems.

No true 1D spin systems exist, yet, so researchers have thus far used quasi-1D systems that approximate 1D dynamics. One such system is crystalline Fluorapatite (FAp) [6, 5]. FAp has its fluorine atoms are arranged in a hexagonal lattice, such that coupling between atoms in a chain is much stronger than that between atoms

in neighboring chains. Due to occasional discontinuities in the crystal, however, the spins at the end of chains have fewer couplings, and thus, a unique spectral signature. Researchers have exploited this to manipulate the ends of chains independently from the spins in the chain [6].

My thesis project can be broken into two pieces. One experimentally investigated the dynamics of multiple quantum coherences in a quasi-1D system under NMR at various angles to the magnetic field. This is important because this is essentially unsimulable; classical computers are unable to accommodate large spin systems, so these investigations cannot be made theoretically.

The second piece investigated the possibility of using rapid rotation of the crystal sample and RF pulses to cancel the effect of off-chain couplings, while leaving in-chain couplings intact. By rotating the sample along the axis of the spin chains, the dynamics of in-chain couplings are scaled, but static with time. The dynamics of off-chain couplings, however, are time-dependent. By further modulating the off-chain couplings with rotation-synchronized RF pulses, I hope to cancel their effect, creating, in effect, a truly 1D spin chain.

Chapter 2

Theory

The tensor is the thing with slots

That perches on the vector.

– Seth Lloyd (with apologies to Emily Dickinson)

2.1 Definitions

First, some definitions. We will make extensive use of the Pauli spin matrices, defined as follows for spin-$\frac{1}{2}$ particles [13]:

$$I_x \equiv \frac{1}{2}\sigma_x \equiv \frac{1}{2}\begin{pmatrix} 0 & 1 \\ 1 & 0 \end{pmatrix} \tag{2.1}$$

$$I_y \equiv \frac{1}{2}\sigma_y \equiv \frac{1}{2}\begin{pmatrix} 0 & -i \\ i & 0 \end{pmatrix} \tag{2.2}$$

$$I_z \equiv \frac{1}{2}\sigma_z \equiv \frac{1}{2}\begin{pmatrix} 1 & 0 \\ 0 & -1 \end{pmatrix} \tag{2.3}$$

$$I_+ \equiv I_x + iI_y \equiv \begin{pmatrix} 0 & 1 \\ 0 & 0 \end{pmatrix} \tag{2.4}$$

$$I_- \equiv I_x - iI_y \equiv \begin{pmatrix} 0 & 0 \\ 1 & 0 \end{pmatrix} \tag{2.5}$$

$$\vec{I} \equiv I_x\hat{x} + I_y\hat{y} + I_z\hat{z} \tag{2.6}$$

We will also make use of the density matrix formalism for quantum mechanics. A system in a pure state $|\psi_i\rangle$ will be represented:

$$\rho_i = |\psi_i\rangle \langle\psi_i| , \tag{2.7}$$

while systems in mixed states will be represented:

$$\rho = \sum_{i=0}^{N} p_i\rho_i = \sum_{i=0}^{N} p_i |\psi_i\rangle \langle\psi_i| , \tag{2.8}$$

where N is the number of such states, and p_i is the probability of a particular state $|\psi_i\rangle$, such that:

$$\sum_{i=0}^{N} p_i = 1. \tag{2.9}$$

2.2 Nuclear Magnetic Resonance

In the presence of a magnetic field, a spin-$\frac{1}{2}$ particle is subject to the following Hamiltonian [20]:

$$\mathcal{H} = -\vec{\mu} \cdot \vec{B}_0, \tag{2.10}$$

where $\vec{\mu} = \hbar\gamma\vec{I}$, $\vec{B}_0$ represents the magnetic field, and γ represents the particle's gyromagnetic ratio. Without loss of generality, we will assume that the magnetic field is in the z-direction:

$$\mathcal{H} = -\hbar\gamma B_0 I_z. \tag{2.11}$$

Thus diagonalized, the Hamiltonian has two eigenstates (also called "eigenspinors"):

$$|\uparrow\rangle \equiv \begin{pmatrix} 1 \\ 0 \end{pmatrix}, \tag{2.12}$$

$$|\downarrow\rangle \equiv \begin{pmatrix} 0 \\ 1 \end{pmatrix}; \tag{2.13}$$

with $|\uparrow\rangle$ called "spin-up" and $|\downarrow\rangle$ called "spin-down."

2.2.1 Evolution of a Single Spin

A single spin can also be in a superposition of these two states; consider:

$$|+\rangle \equiv \frac{1}{\sqrt{2}}\left(|\uparrow\rangle + |\downarrow\rangle\right), \tag{2.14}$$

$$|-\rangle \equiv \frac{1}{\sqrt{2}}\left(|\uparrow\rangle - |\downarrow\rangle\right); \tag{2.15}$$

the eigenstates of the I_x operator, equivalent to a spin the the positive x-direction and negative x-direction. How will such a state evolve? We can compute the answer:

$$\begin{aligned} |\psi(t)\rangle &= e^{-\frac{i\mathcal{H}t}{\hbar}}|+\rangle = e^{i\gamma B_0 I_z t}|+\rangle = \left[\cos(\gamma B_0 t) + i\sin(\gamma B_0 t) I_z\right]|+\rangle \\ |\psi(t)\rangle &= \cos(\gamma B_0 t)|+\rangle + i\sin(\gamma B_0 t)|-\rangle . \end{aligned} \tag{2.16}$$

Thus such states will precess around the z-axis with angular frequency:

$$\omega_L = \gamma B_0, \tag{2.17}$$

called the Larmor frequency.

Still, how are we to manipulate this system? The answer is through radiofrequency (RF) radiation. To examine how the system evolves under such radiation, let us start with the Hamiltonian in the lab frame, with the wave's magnetic field amplitude set

to B_1, and its angular frequency set to ω:

$$\mathcal{H}_{lab} = -\hbar\gamma B_0 I_z - \hbar\gamma B_1 \cos(\omega t) I_x. \tag{2.18}$$

It will be more convenient to decompose the field into two rotating elements as follows:

$$\begin{aligned}\mathcal{H}_{lab} = -\hbar\gamma B_0 I_z - \frac{\hbar\gamma B_1}{2} &[(\cos(\omega t) I_x + \sin(\omega t) I_y) \\ &- (\cos(\omega t) I_x - \sin(\omega t) I_y)]\,.\end{aligned} \tag{2.19}$$

Now let us define a rotating frame, rotating clockwise about the x-axis at angular frequency ω:

$$I_{x'} \equiv e^{-i\omega t I_z} I_x e^{i\omega t I_z} = \cos(\omega t) I_x + \sin(\omega t) I_y \tag{2.20}$$

$$I_{y'} \equiv e^{-i\omega t I_z} I_y e^{i\omega t I_z} = -\sin(\omega t) I_x + \cos(\omega t) I_y \tag{2.21}$$

$$I_{z'} \equiv e^{-i\omega t I_z} I_z e^{i\omega t I_z} = I_z \tag{2.22}$$

and define the wavefunction in the rotating frame:

$$|\psi_{rot}(t)\rangle = e^{i\omega t I_z} |\psi(t)\rangle\,. \tag{2.23}$$

Using the Schödinger equation:

$$i\hbar \frac{d|\psi(t)\rangle}{dt} = \mathcal{H}_{lab} |\psi(t)\rangle \tag{2.24}$$

$$i\hbar \frac{d|\psi_{rot}(t)\rangle}{dt} + \hbar\omega I_z |\psi_{rot}(t)\rangle = e^{i\omega t I_z} \mathcal{H}_{lab} e^{-i\omega t I_z} |\psi_{rot}(t)\rangle\,, \tag{2.25}$$

we are led naturally to define a new Hamiltonian in the rotating frame:

$$\mathcal{H}_{rot} = e^{i\omega t I_z} \mathcal{H}_{lab} e^{-i\omega t I_z} - \hbar\omega I_z, \tag{2.26}$$

and recalling Equation 2.19, we compute this new Hamiltonian:

$$\mathcal{H}_{rot} = -\left(\hbar\omega_L + \hbar\omega\right) I_z - \frac{\hbar\gamma B_1}{2}\left[I_x - e^{i2\omega t I_z} I_x e^{-i2\omega t I_z}\right]. \tag{2.27}$$

The terms rotating at angular frequency 2ω have an existent, but for our purposes, negligible [20] effect; interested readers are advised to refer to Mehring's explanation of Bloch-Siegert oscillations [17]. Thus neglecting it:

$$\mathcal{H}_{rot} = -\left(\hbar\omega_L + \hbar\omega\right) I_z - \frac{\hbar\gamma B_1}{2} I_x \tag{2.28}$$

Again, our aim should be immediately apparent; when at resonance, that is, $\omega = -\omega_L$, the Hamiltonian becomes:

$$\mathcal{H}_{rot} = -\frac{\hbar\gamma B_1}{2} I_x \tag{2.29}$$

What effect have we achieved? By applying a sinusoidal field, we are able to "nutate" the polarization about the x-axis, just as a static field causes a spin to precess.

One should also note that we are not restricted to the x-axis; by altering the phase of our waves by just 90°, we can just as easily arrive at:

$$\mathcal{H}_{rot} = -\frac{\hbar\gamma B_1}{2} I_y \tag{2.30}$$

Pulses

One particular application of this is pulses which nutate the polarization some precise angle, for instance, exactly $90° = \frac{\pi}{2}$ radians. By choosing time $t_{\frac{\pi}{2}} = \frac{\pi}{\gamma B_1}$, and irradiating the particle with RF for precisely that time, we will apply a unitary operator:

$$R_x\left(\frac{\pi}{2}\right) = e^{-i\frac{\gamma B_1}{2} t_{\frac{\pi}{2}} I_x} = e^{-i\frac{\pi}{2} I_x} = -iI_x. \tag{2.31}$$

Such pulses are very important for quantum computing.

2.2.2 Evolution of Multiple Spins

Systems with multiple spins are somewhat more complicated. To deal with the presence of multiple spins, we will now address them, for instance using operator I_{zi} to represent the z-axis spin operator applied to the ith spin. Unaddressed spin operators, for instance, I_z will now refer to collective spin operators:

$$I_z = \sum_{i=0}^{N} I_{zi} \tag{2.32}$$

In addition to the familiar precession term, we must now add several dipolar terms:

$$\mathcal{H}_{rot} = -\hbar\gamma B_0 I_z + \sum_{i>j} \frac{\hbar^2\gamma^2}{2r_{ij}^3}\left(1 - 3\cos^2\theta_{ij}\right)\left(3I_{zi}I_{zj} - \vec{I}_i \cdot \vec{I}_j\right), \tag{2.33}$$

where r_{ij} is the distance between the ith and jth spins, and θ_{ij} is the angle they make with magnetic field (which we have designated the z-axis). These dipolar couplings can be exploited in order to entangle the two particles.

2.3 Effect of Radiation on Dipolar Couplings

Another important effect is that of alternating fields on dipolar couplings [20]. Let us return to Equation 2.33, and consider the addition of an alternating magnetic field:

$$\begin{aligned}\mathcal{H}_{rot} &= -\left(\hbar\gamma B_0 - \hbar\omega\right) I_z - \frac{\hbar\gamma B_1}{2} I_x \\ &\quad + \sum_{i>j} \frac{\hbar^2\gamma^2}{2r_{ij}^3}\left(1 - 3\cos^2\theta_{ij}\right)\left(3I_{zi}I_{zj} - \vec{I}_i \cdot \vec{I}_j\right),\end{aligned} \tag{2.34}$$

We will represent the new effective magnetic field in the rotating frame as:

$$B_{eff} = \left(B_0 - \frac{\omega}{\gamma}\right)\hat{z} + \frac{B_1}{2}\hat{x} \tag{2.35}$$

$$\theta = \arctan\left(\frac{B_1}{2\left(B_0 - \frac{\omega}{\gamma}\right)}\right), \tag{2.36}$$

where θ is the angle it makes with the z-axis.

At this point, we will define a new coordinate system, one that is pointing along the axis of the effective field. We will represent this new system with capital letters:

$$I_Z = \cos(\theta)I_z + \sin(\theta)I_x \tag{2.37}$$

$$I_X = -\sin(\theta)I_z + \cos(\theta)I_x \tag{2.38}$$

$$I_Y = I_y. \tag{2.39}$$

Substituting these operators, we arrive at:

$$\begin{aligned}
\mathcal{H}_{rot} = & -\hbar\gamma B_{eff} I_Z \\
& + \frac{1}{2}\left(3\cos^2\theta - 1\right)\sum_{i>j} A_{ij}\left(3I_{Zi}I_{Zj} - \vec{I}_i \cdot \vec{I}_j\right) \\
& + \left[-\frac{3}{2}\sin\theta\cos\theta\sum_{i>j} A_{ij}\left(I_{+i}I_{Zj} + I_{Zi}I_{+j}\right)\right. \\
& -\frac{3}{2}\sin\theta\cos\theta\sum_{i>j} A_{ij}\left(I_{-i}I_{Zj} + I_{Zi}I_{-j}\right) \\
& \left. -\frac{3}{4}\sin^2\theta\sum_{i>j} A_{ij}\left(I_{+i}I_{+j}\right) - \frac{3}{4}\sin^2\theta\sum_{i>j} A_{ij}\left(I_{-i}I_{-j}\right)\right]
\end{aligned} \tag{2.40}$$

defining for our convenience:

$$A_{ij} = \frac{\hbar^2\gamma^2}{2r_{ij}^3}\left(1 - 3\cos^2\theta_{ij}\right) \tag{2.41}$$

Note that the terms in the square brackets do not commute with the Zeeman interactions of the effective field; thus, as a first approximation we can ignore them.

Thus we arrive at the Lee-Goldburg technique [12]. While Lee and Goldburg concentrated on tuning the system to the magic angle, $\theta = \arccos\sqrt{\frac{1}{3}}$, in order to destroy the dipolar coupling entirely, Barnaal and Lowe instead investigated its effects

at resonance, with $\theta = 90°$ [3]. At resonance, the equation becomes:

$$\mathcal{H}_{rot} = -\hbar\gamma B_{eff} I_Z - \frac{1}{2}\sum_{i>j} A_{ij}\left(3I_{Zi}I_{Zj} - \vec{I}_i \cdot \vec{I}_j\right) \tag{2.42}$$

Thus, we have multiplied the dipolar coupling terms by $-\frac{1}{2}$, in our new effective field coordinate system. If we now consult Equation 2.37 and convert back to our original coordinate system, we arrive at:

$$\mathcal{H}_{rot} = -\hbar\gamma B_{eff} I_x - \frac{1}{2}\sum_{i>j} A_{ij}\left(3I_{xi}I_{xj} - \vec{I}_i \cdot \vec{I}_j\right) \tag{2.43}$$

Magic Echoes

The factor of $-\frac{1}{2}$ in front of the dipolar coupling terms is very important. In fact, it can lead to a method of reversing the dipolar evolution, called *magic echoes*. First, let us label the dipolar Hamiltonians:

$$\begin{aligned}
\mathcal{H}_{xx} &= \sum_{i>j} A_{ij}\left(3I_{xi}I_{xj} - \vec{I}_i \cdot \vec{I}_j\right) \\
\mathcal{H}_{yy} &= \sum_{i>j} A_{ij}\left(3I_{yi}I_{yj} - \vec{I}_i \cdot \vec{I}_j\right) \\
\mathcal{H}_{zz} &= \sum_{i>j} A_{ij}\left(3I_{zi}I_{zj} - \vec{I}_i \cdot \vec{I}_j\right)
\end{aligned} \tag{2.44}$$

Using Average Hamiltonian Theory [20], it is possible to show that, in fact:

$$R_y\left(\frac{\pi}{2}\right)\mathcal{H}_{xx}R_y\left(-\frac{\pi}{2}\right) = \mathcal{H}_{zz}, \tag{2.45}$$

or in other words, by preceding our radiation with a negative 90° Y pulse, and following it with a positive 90° Y pulse, we return to the correct dipolar Hamiltonian, $\mathcal{H}_{zz}$. Thus, by letting a system evolve for time τ, then hitting it with a negative 90° Y pulse, letting it evolve under constant radiation for 2τ, and hitting it with a positive 90° Y pulse, we cancel all dipolar evolution. This technique, created by Rhim and Kessemeier [19, 14], then subsequently explained by Rhim, Pines, and Waugh [18], is

called a "magic echo."

2.4 Multiple Quantum Coherences

In NMR, we can easily observe coherences involving only one spin. But this only paints a small part of the full picture—what of those involving many spins? We then define an n-quantum coherence as a transition between two states such that the change in energy, ΔE is equal to $n\hbar\omega$, or n quanta [20].

What are some examples? Zero-quantum terms are not transitions at all, unless the system is degenerate; thus, they are represented by on-diagonal terms only. One-quantum terms are those arising when the system is polarized, as by a 90° pulse:

$$\rho_1 = R_x\left(\frac{\pi}{2}\right) I_z R_x\left(-\frac{\pi}{2}\right) = I_y \tag{2.46}$$

$$\rho_2 = R_y\left(\frac{\pi}{2}\right) I_z R_y\left(-\frac{\pi}{2}\right) = -I_x \tag{2.47}$$

However, to be precise, these two are combinations of the "raising" (I_+) and "lowering" (I_-) operators (Equation 2.4–2.5):

$$I_x = \frac{1}{2}(I_+ + I_-) \tag{2.48}$$

$$I_y = -\frac{i}{2}(I_+ - I_-) \tag{2.49}$$

Two-quantum terms are necessarily more wily; they involve two spins. As it turns out, terms are two-quantum if they are the tensor product of two raising or two lowering operators:

$$I_+ \otimes I_+ = |00\rangle\langle 11| \tag{2.50}$$

$$I_- \otimes I_- = |11\rangle\langle 00|, \tag{2.51}$$

while the tensor products of two opposite operators:

$$I_+ \otimes I_- = |01\rangle\langle 10| \tag{2.52}$$

$$I_- \otimes I_+ = |10\rangle\langle 01| \tag{2.53}$$

remain stubbornly zero-quantum. This pattern continues to hold; the degree of a term's multiple-quantum coherence is determined by the sum of all its raising and lowering operators; for example:

$$\rho = I_+ \otimes I_z \otimes I_- \otimes I_- \otimes I_+ \otimes I_+ \otimes I_+ \otimes I_+ \otimes I_z \tag{2.54}$$

is a 3-quantum coherence.

Still, how are we to observe such terms? The answer, as it so often is in NMR, is "with another pulse sequence."

2.4.1 The Multiple-Quantum Pulse Sequence

First, let us examine the action of multiple-quantum coherences under z-rotation:

$$e^{-i\frac{\theta}{2}I_z} I_+ e^{i\frac{\theta}{2}I_z} = e^{-i\theta} I_+ \tag{2.55}$$

$$e^{-i\frac{\theta}{2}I_z} I_- e^{i\frac{\theta}{2}I_z} = e^{i\theta} I_- \tag{2.56}$$

Readers suspecting we are about to bring tensor products into the mess would be correct. This property of the raising and lowering operators continues to apply, meaning that for n-quantum term ρ_n:

$$e^{-i\frac{\theta}{2}\bigotimes_i I_{zi}} \rho_n e^{i\frac{\theta}{2}\bigotimes_i I_{zi}} = e^{-in\theta}\rho_n \tag{2.57}$$

We can use this effect in order to distinguish different coherences, then use refocusing techniques to return them to observable states.

Our main tool in this endeavor will be the 8-pulse double-quantum sequence:

$$\frac{\tau}{2} - X - 2\tau - X - \tau - X - 2\tau - X - \tau - \bar{X} - 2\tau - \bar{X} - \tau - \bar{X} - 2\tau - \bar{X} - \frac{\tau}{2} \tag{2.58}$$

Under this pulse sequence, a system will be caused to evolve under the so-called "double quantum" Hamiltonian,

$$\mathcal{H}_{DQ} = \sum_{i>j} A_{ij} I_{+i} I_{+j} + I_{-i} I_{-j}, \tag{2.59}$$

acquiring high-order quantum coherences along the way. Next, we apply the inverse of this, but with its phase altered by ϕ [4], and finally a $\frac{\pi}{2}$ pulse:

$$U_{re} = e^{\left(-i\frac{\pi}{4}\sum_k I_{yk}\right)} U'_{MQC} = e^{\left(-i\frac{\pi}{4}\sum_k I_{yk}\right)} e^{\left(i\frac{\phi}{2}\sum_k I_{zk}\right)} U^{\dagger}_{MQC} e^{\left(-i\frac{\phi}{2}\sum_k I_{zk}\right)} \tag{2.60}$$

which has readout signal:

$$S = \sum_p Tr\left[e^{ip\phi}\rho_p^2\right]. \tag{2.61}$$

By observing of all angles ϕ between 0 and 2π in M evenly spaced steps, then taking the Fourier transform, we can distinguish coherences up to order M.

Chapter 3

Equipment

3.1 Apparatus

The spectrometer used was a Bruker Avance 300 spectrometer. Data was collected using XWIN-NMR 3.5 on a Dell PC running Red Hat Linux 7. Most pulse sequence scripts used were written by Paola Cappellaro, with the exception of the Fidelity Decay sequence, written by Natania Antler, and one of the Solid Echo scripts, written by Chandrasekhar Ramanathan.

The probe was of custom design, created by Chandrasekhar Ramanathan and Peter Allen. I helped Peter Allen modify the probe head to allow precise rotation to a particular angle, and to allow us to swap the liquid sample and the solid sample. The new probe head consists of a glass sample tube placed within the RF coil, with a notched wheel attached to it. By inserting the sample into this tube, lining it up, and then turning the wheel, one can repeatably rotate the sample to a particular angle (to within about 5°). Figure 3-1 shows the modified probehead, with a solid sample inserted and turned to 55°.

3.1.1 Fluorapatite Crystal

The Fluorapatite (FAp) crystal was grown by Prof. Ian Fisher of Stanford. FAp (Figure 3-2) has chemical formula $Ca_5(PO_4)_3F$. FAp is a hexagonal crystal lattice.

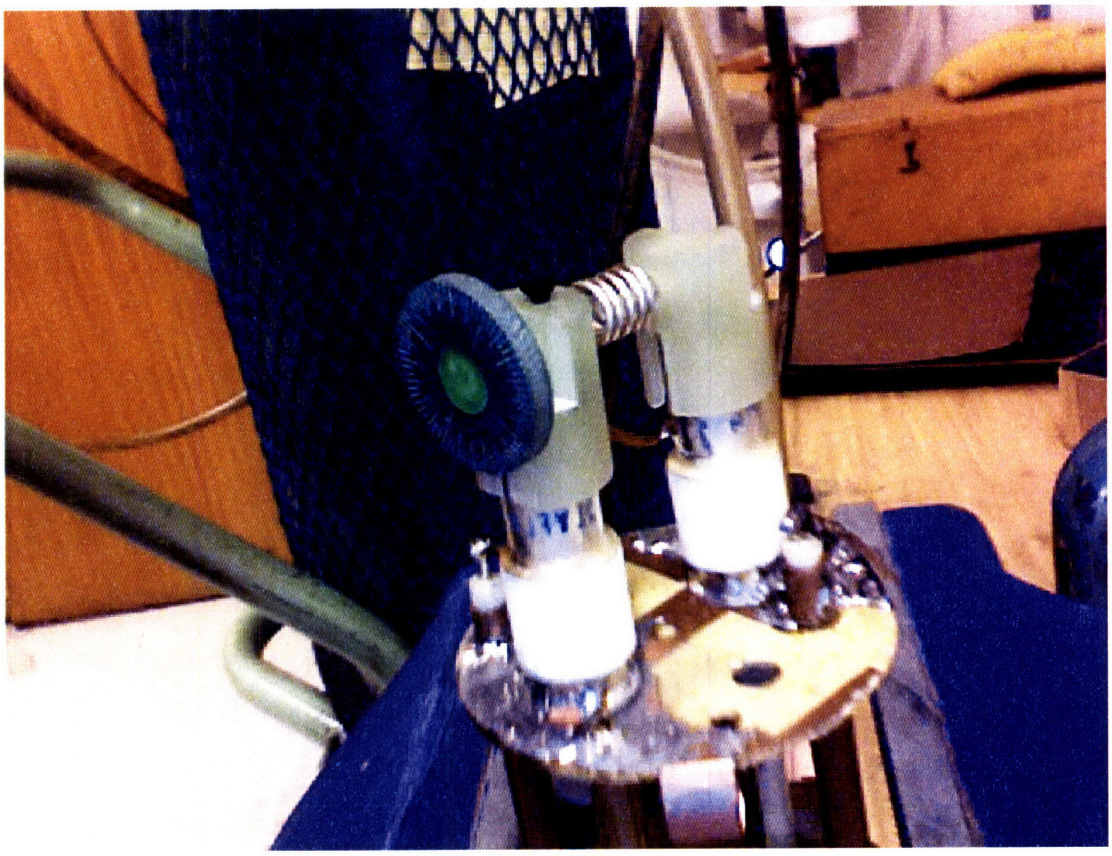

Figure 3-1: The modified probe head, with a Fluorapatite sample oriented at 55°

Its basic unit cell has $a = 9.40$Å and $c = 6.88$Å.Thus, off-chain spins are separated by 9.40Å, while on-chain spins are separated by 3.44Å. As a result of Equation 2.33, off-chain couplings act on a timescale nearly 20 times longer than on-chain couplings. FAp has thus been called a "quasi-1D" system.

This quasi-1D nature has made FAp the object of numerous NMR studies [8, 7, 11]. It also makes FAp an excellent candidate for spin transport [6] and Quantum Information Processing [4, 5].

3.2 Calibration

The general idea of calibrating the system was to tune the cavity to the correct frequency, then optimize 90° pulse widths using a liquid sample of fluorocyclohexane ($C_6H_{11}F$). Following this step, the probe was carefully removed from the spectrometer, and the liquid sample was replaced with the solid sample, aligned to the angle desired using the modified probe head. Next, we verified that the cavity tuning had not been altered by an errant bump of the highly sensitive tuning rods. Finally, we performed solid echo experiments to verify the angle of orientation of the crystal. In this section we will discuss the calibration in more detail.

3.2.1 Cavity Tuning

The first step in calibration was cavity tuning. The probe had three tuning rods, one for gross adjustment of frequency, one for fine adjustment of freqency, and one for adjustment of matching. Though one would think our goal was perfect alignment in both frequency and matching, in reality this was not the case. Matching needed to be very slightly off, due to our fast pulse times. If matching was too perfect, we observed strong ring-down effects preventing proper execution of the flip-flop pulse sequence.

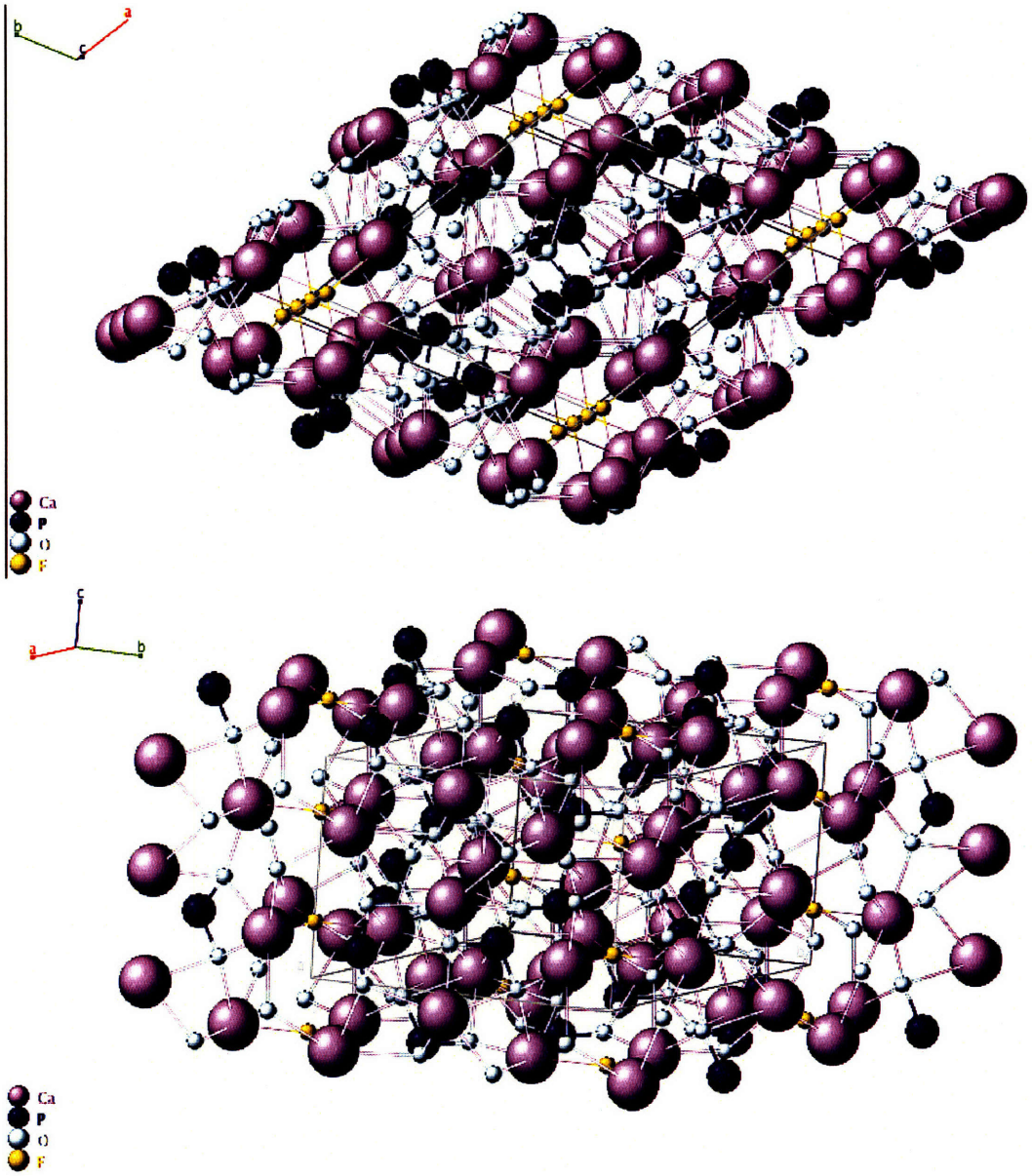

Figure 3-2: Crystal structure of Fluorapatite (Created with jPOWD, by Mineral Data, Inc). **Top**: Overhead view. **Bottom**: Side view

3.2.2 The 90°-90° Pulse Sequence

The 90°-90° pulse sequence (`pc.90pls`, originally created by Paola Cappellaro), was used to arrive at the perfect width for a 90° pulse on fluorine atoms. The pulse sequence was executed with a liquid sample of fluorocyclohexane, due to the prohibitively long relaxation times of the solid sample. The pulse sequence consisted of 500 repeated pulses at a particular power level (`pl2`) and duration (`p1`), with continuous observation of the polarization.

Even small deviations from the correct width were readily apparent; after several pulses the polarization would begin to decay. Adjustment required tenacity and trial-and-error; due to the granularity of the adjustable parameters, I often had to try many combinations, and sometimes even a new cavity tuning before arriving at an acceptable pulse width. Due to the enormous number of pulses present in running the MQC24 sequence for any significant amount of time, the pulse widths needed to be as accurate as possible. Figure 3-3 shows the results of a correctly aligned sequence.

3.2.3 The "Flip-flop" Pulse Sequence

After arriving at a reasonable pulse width, I would apply the flip-flop pulse sequence (`pc.ff2`, also created by Paola Cappellaro) to verify that there were not issues with the phase. This sequence applied a 90° pulse, followed by a $-90°$ pulse, for 500 cycles. The goal of this pulse sequence was to confirm that there were no ring-down effects present from the matching being too perfectly tuned.

In practice, I would run this sequence on loop while performing active adjustments to the tuning rods. Changes were immediately visible in the XWIN-NMR display, and I would adjust the rods until I reached a reasonable setting.

At this point, I would return to the `pc.90pls` sequence, since any major changes in the tuning would alter the correct pulse width. Generally I would need to perform a few cycles of each sequence in order to finally arrive a tuning and pulse width that satisfied both.

Figure 3-3: Signal of a 90°-90° pulse sequence with properly calibrated pulse width

3.2.4 Swapping Samples

At this point, it was time to put in the solid sample. Extremely carefully, avoiding jostling the sensitive tuning rods, I would remove the probe from the spectrometer and move it to a vice grip. At this point, I would remove the liquid sample, setting it aside, and replace it with the FAp crystal. I would use the notched wheel to orient the crystal at the angle we wished to study. Then I carefully replaced the probe in the NMR spectrometer. Finally, I re-checked the cavity tuning to confirm that any changes were minimal.

3.2.5 Solid Echoes

At this point, I would perform Solid Echo experiments (`pc.SolidEcho`, by Paola Cappellaro, and `cr.T1filtSolidEcho`, by Chandrasekhar Ramanathan) in order to verify the angle of orientation. It is known that the bandwidth of the solid echo corresponds to its angle. A typical solid echo experiment is shown in Figure 3-4.

Further, the Solid Echo experiment could be used to verify the pulse width calibration: at a pulse width of 180°, the solid echo is expected to have 0 amplitude. Thus, in some of the experiments with the crystal aligned at the magic angle (Section 4.2.2), which required longer evolution times, we performed Solid Echoes using a number of durations (`p1`) of approximately twice our calculated pulse width in order to check this.

3.3 Fidelity Decay

Lastly, before beginning experiments, I performed Fidelity Decays (`na.FidelDecay`, written by Natania Antler). This involved running the MQC-24 pulse sequence for up to 35 loops using various delays, and determining with what fidelity the original state remained. I used this data to determine how many loops and how long of delays were acceptable before we began to lose accuracy due to the high number of pulses.

Due to the combination of long relaxations times, extra runs needed for sym-

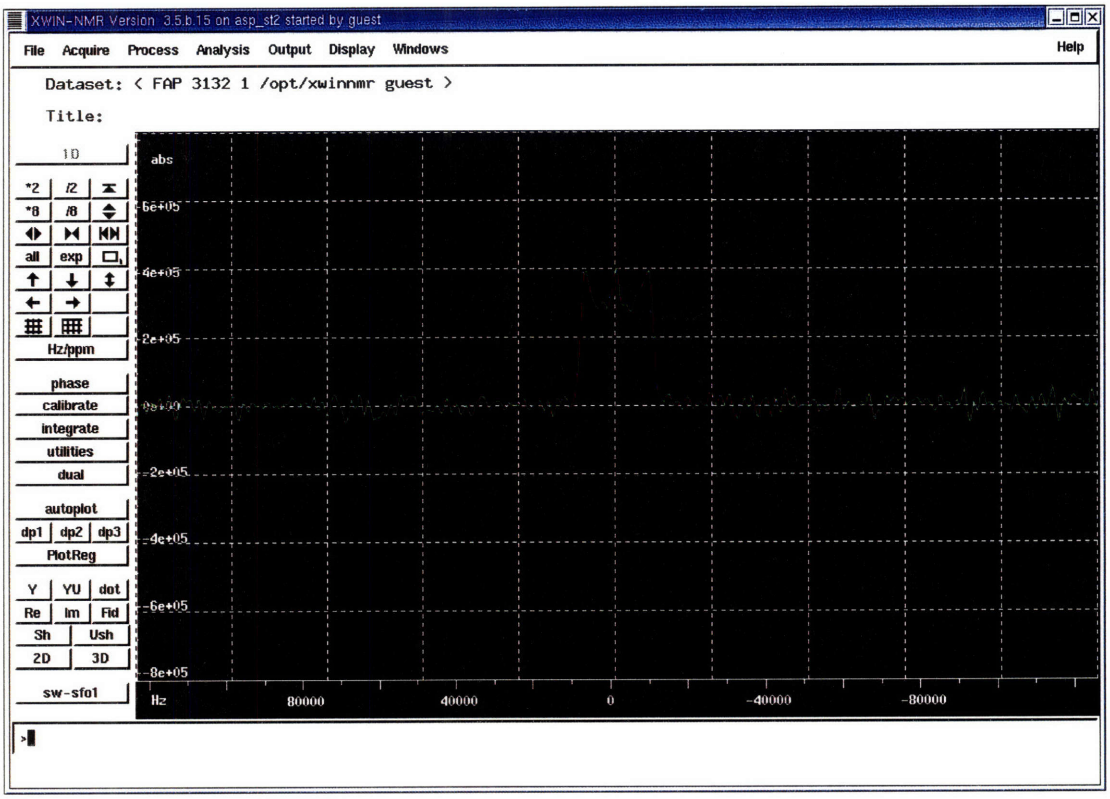

Figure 3-4: Fourier transform of a typical T1-filtered solid echo, with the system aligned with the field ($\theta = 0°$)

metrization, and high number of experiments, these sequences were run over the course of several days.

Chapter 4

MQC Dynamics Under Angular Rotation

In this section, I will present the results of my experiments involving MQC dynamics at different angular orientations. I will begin with the simulations motivating my choice of angles to study, then proceed to the actual results of those experiments. Finally, I will discuss the correspondence of my results with predictions and with prior results using similar methods.

4.1 Simulations

To begin, my goal was to explore what angles were likely to yield interesting dynamics. To this end, I performed a number of simulations of the dynamics of systems involving 6 spins to get an idea for which angles to explore.

The reason for selecting 6 spins was merely one of computational power. Each additional spin doubles both dimensions of the matrices involved in simulating such systems. Thus, classical computers have much difficulty simulating the dynamics of systems involving many spins. Many-spin systems often require sparse-matrix techniques [10] and systems of more than about 30 are nearly impossible to explore, even with the use of supercomputers. I settled on 6 as a number of spins manageable with basic software like MATLAB, yet large enough to contain relevant formations.

I started by creating a robust simulation program (see Appendix A) capable of simulating the dynamics of any measurement operator on a system evolving under the dipolar Hamiltonian (Equation 2.33). Then I picked simulations.

4.1.1 Chain with off-chain elements

I began by considering a chain of 4 spins with 2 off-chain elements in the plane of the two center spins. To make the system more FAp-like, I increased the distance between on- and off-chain elements to be three times that of on-chain elements from their nearest neighbor. This makes the system more quasi-1D. The precise layout of spins is pictured in Figure 4-1. This layout is similar to FAp in that it allows us to determine when multiple-quantum coherences develop between off-chain terms, and what angles are likely to alter this.

Then, I simulated the system's evolution, rotating the chain to various angles between 0° and 90° about the x-axis. The results can be seen in Figure 4-1. In this we noted interesting and characteristic dynamics at the on-field angle, $\theta = 0°$, and at the magic angle $\theta \approx 54.7°$ (described in more detail in Section 5.1); other angles seemed to be time-scaled versions of the on-chain dynamics.

4.1.2 Hexagon

Next, I simulated a hexagon of spins in the orientation shown in Figure 4-2. This system was also relevant to studying FAp, since it represents the hexagonal pattern repeating in FAp. With this simulation, we also hoped to get a sense of what to look for in the experiments oriented at the magic angle, since with the on-chain coupling destroyed, the strongest couplings would now be the off-chain hexagonal ones.

As before, I simulated the system's evolution, rotating the hexagon to various angles between 0° and 90° about the x-axis. The results can be seen in Figure 4-2. Again, $\theta = 0°$ and $\theta = 54.7°$ had the most striking dynamics, as well as $\theta \approx 40°$ and $\theta = 90°$

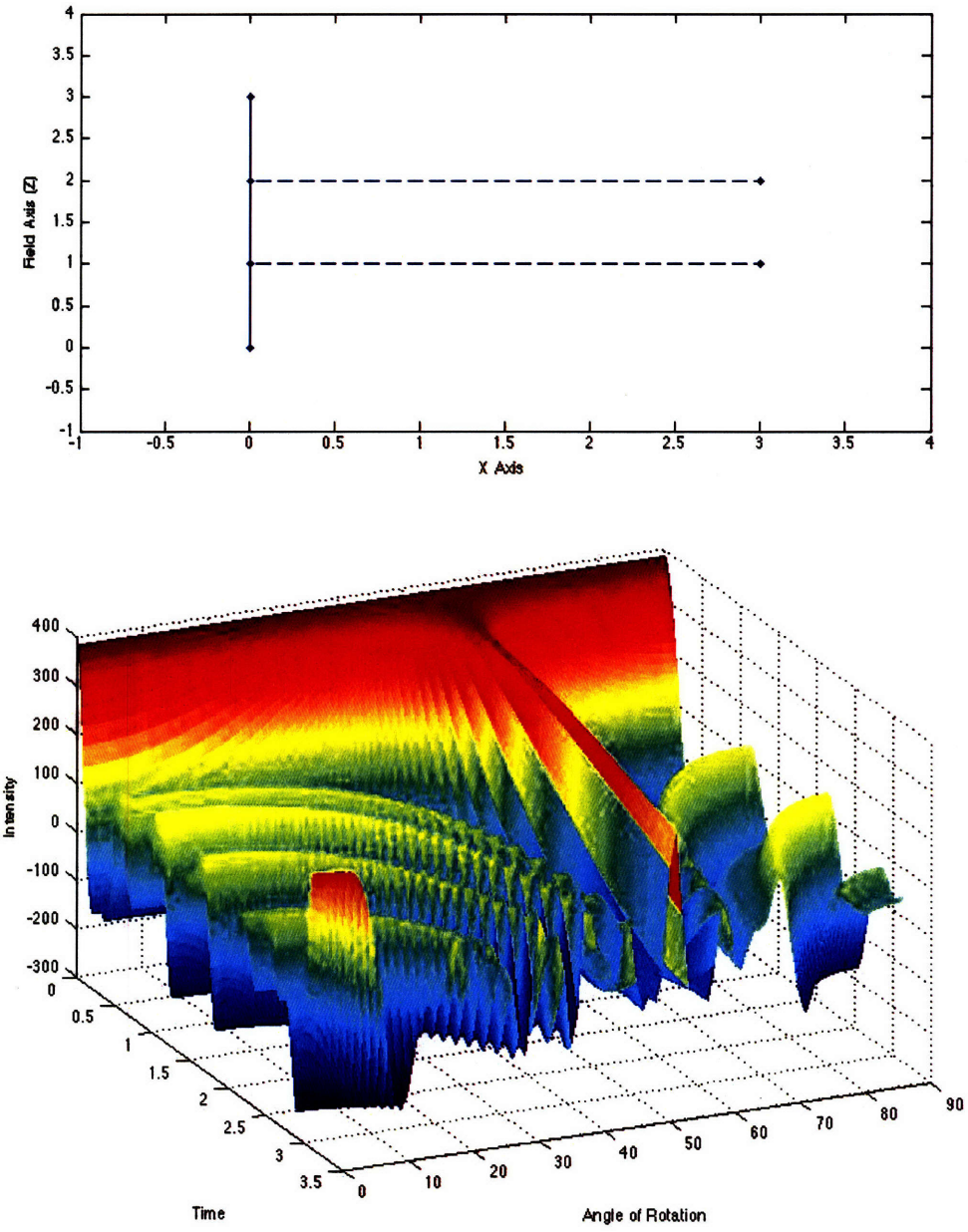

Figure 4-1: **Top**: Orientation of spins. **Bottom**: 3D plot of total x-polarization of chain of four spins with two off-chain spins, oriented at different angles following 90° pulse.

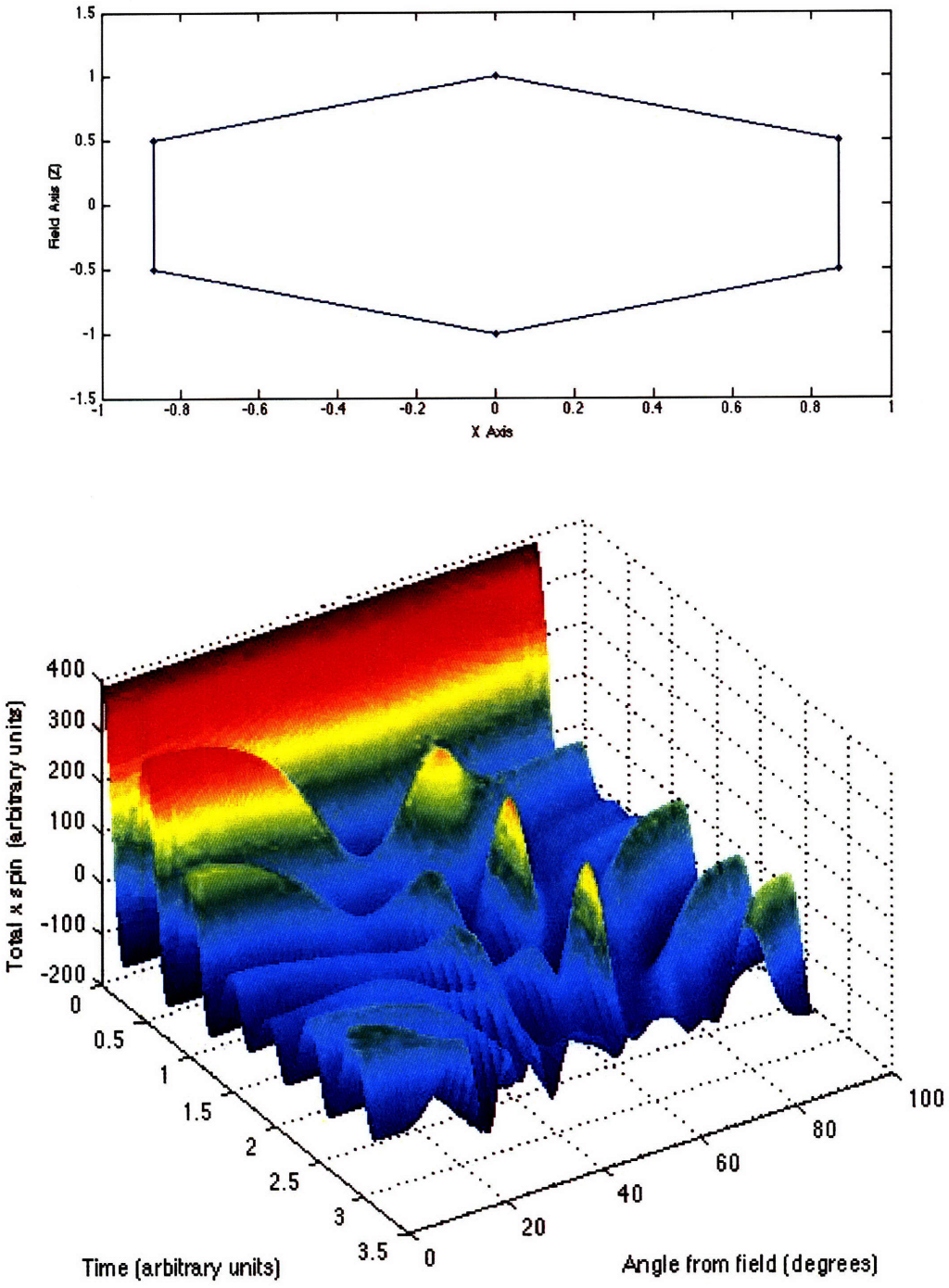

Figure 4-2: **Top**: Orientation of spins. **Bottom**: 3D plot of total x-polarization of hexagon of spins at different angles following 90° pulse.

4.2 Experiments

Based on these results, we opted to do experiments at $\theta = 0°$ and $\theta = 54.7°$. The experiments were performed using the NMR Spectrometer described in Chapter 3. After calibrating the spectrometer and inserting the FAp crystal as oriented at the proper angle, we performed experiments using the Multiple Quantum pulse sequence, with 24 different phases so as to distinguish coherences -12 through 11, and then Fourier transformed to determine the strength of each coherence.

4.2.1 On-axis Dynamics

The results for the crystal aligned with the field ($\theta = 0°$) are presented in Figure 4-3. As expected, they show much correspondence with the results of [4], which had

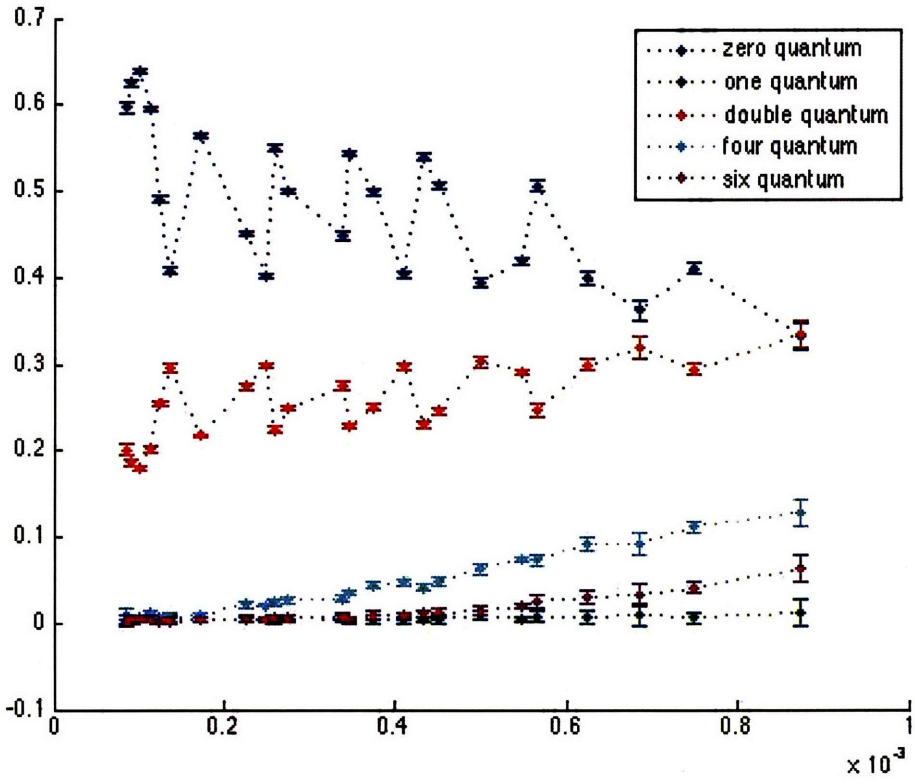

Figure 4-3: The evolution of multiple quantum coherences in Fluorapatite at $\theta = 0°$. Time is in seconds. The strongest coupling has a period of $1.91e-4$ seconds.

performed a similar experiment, though with only 16 phases. That said, they do not show one of its most interesting features: the 0-coherences do not exhibit a sudden trend downwards or upwards, and the oscillations occur more slowly, indicating a chain length significantly higher than 11 spins,

As expected, no significant odd-quantum coherences are observed, even at high times; this indicates that our pulse widths are accurate.

4.2.2 Magic Angle Dynamics

The magic angle dynamics are more interesting, since they have not been probed before. The results are shown in Figure 4-4. As expected, they show very slow evolution and primarily remain 0-quantum. However, unexpectedly, they do not show evolution even as we begin to approach the length of a period of their strongest coupling (.0077s).

It is likely that more experiments need to be done to determine how the system evolves beyond this time, since we were only able to reach about .7 times the duration of the period of the strongest coupling. However, this will present new experimental challenges, as this will either require a major increase in the delay (τ) of the multiple quantum sequence, or in the number of loops of the multiple quantum sequence. To increase the number of loops may require an increase in the accuracy of the 90° pulse.

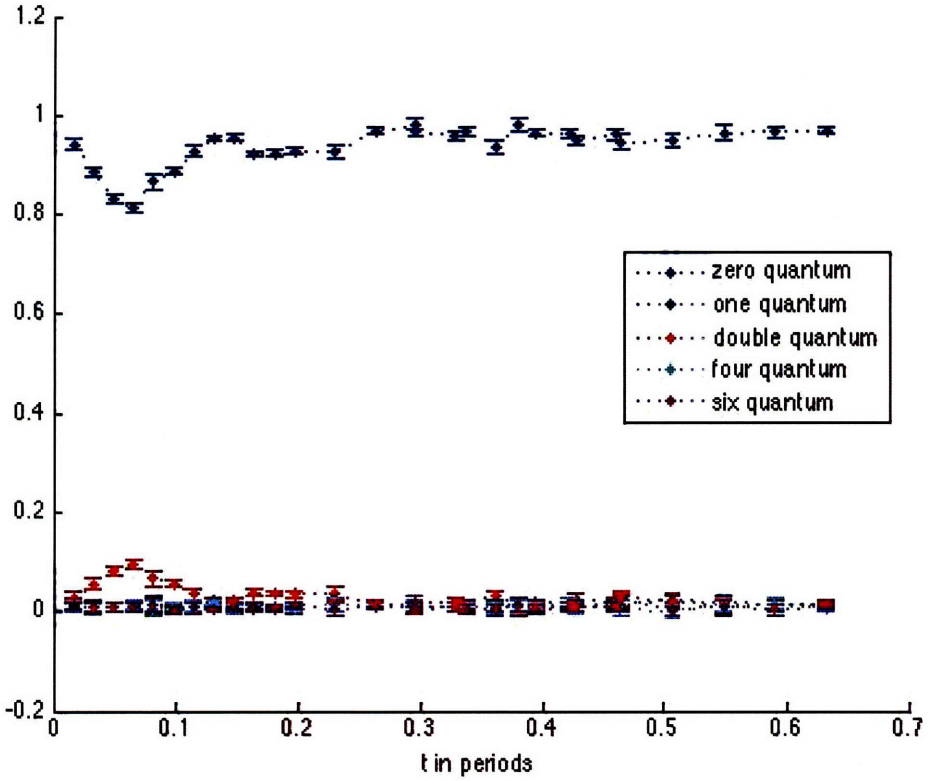

Figure 4-4: The evolution of multiple quantum coherences in Fluorapatite at $\theta = 55°$. Time is in periods of the strongest coupling (.0077 seconds).

Chapter 5

Cancelling Unwanted Couplings Using Magnetic-resonance Behavior, Emission, and Rotation

One problem with NMR techniques is that many studies have been performed on the theoretical dynamics of a 1D spin chain, and yet there is no good way to realize this system experimentally. Quasi-1D systems like Fluorapatite are an excellent start, but the off-chain dynamics quickly become relevant. Thus, I set out to create a technique to selectively cancel some couplings, while preserving others. In this way we could cancel the off-chain couplings, while preserving the on-chain couplings, and realize a "truly" 1D system.

5.1 Framework

But how to do it? The framework I arrived at combines the ideas of magic angle spinning with those of magic echoes.

Magic angle spinning is a well-known NMR technique, discovered independently by Lowe [16], and Andrew, et al. [1, 2]. In Equation 2.33, we can see that the factor of $(1 - 3\cos^2(\theta_{ij}))$ will yield one particular angle, the magic angle ($\theta_{ij} = \arccos\left(\frac{1}{\sqrt{3}}\right) \approx 54.7°$), at which the dipolar coupling will be cancelled. In fact, we can do better;

by rotating the system about an axis at this angle (Figure 5-1), we will cancel all couplings to zeroth order in Average Hamiltonian Theory.

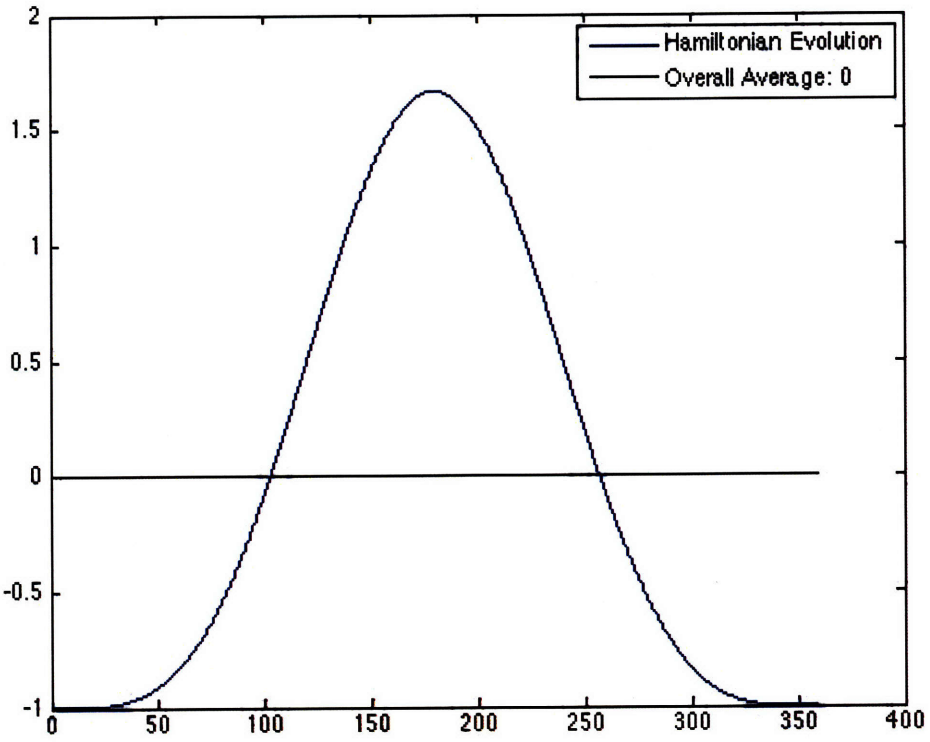

Figure 5-1: Magnitude of on-chain coupling under magic angle spinning

Still, there is no obvious way to make some couplings average to zero while others do not. But now, looking at equation describing dipolar evolution under radiation, Equation 2.42, one is struck by the ability to "reverse" the evolution of the dipolar Hamiltonian. It also allows us to make the Hamiltonian negative at certain times by using a long period of radiation (much longer than a pulse). Since different couplings will have different evolutions under rotation at the same angle, we can optimize and find a way to cancel certain couplings while preserving others.

5.2 Searching for Solutions

Thus, our search begins. I wrote some MATLAB code (Appendix B) to use `fmincon` to attempt to maximize the average of the dipolar Hamiltonian for on-chain couplings, under the nonlinear constraint that the off-chain couplings in the same plane as the spin at angles of $\phi = \{0°, 120°, 240°\}$ were cancelled.

The best solution I arrived at diminished all three undesirable couplings to about 9 orders of magnitude, while only diminishing the on-chain coupling to about a fifth of it initial value. This scheme involved orienting the crystal along an angle of $\theta = 10.3°$ from the magnetic field, and then rotating it about an angle $\theta_r = 31.1°$ from the magnetic field. During this uniform rotation, there is one long RF pulse, lasting from the time where we rotate through $\psi = 312.7°$ until the time where we rotate through $\psi = 94.7°$.

Figure 5-2 shows the evolution of the on-chain coupling under this scheme, while Figure 5-3 confirms that off-chain couplings are destroyed. The blue line represents the normal dipolar Hamiltonian, while the thick red line represents the Hamiltonian with a factor of $-\frac{1}{2}$ in front during the portions under RF radiation.

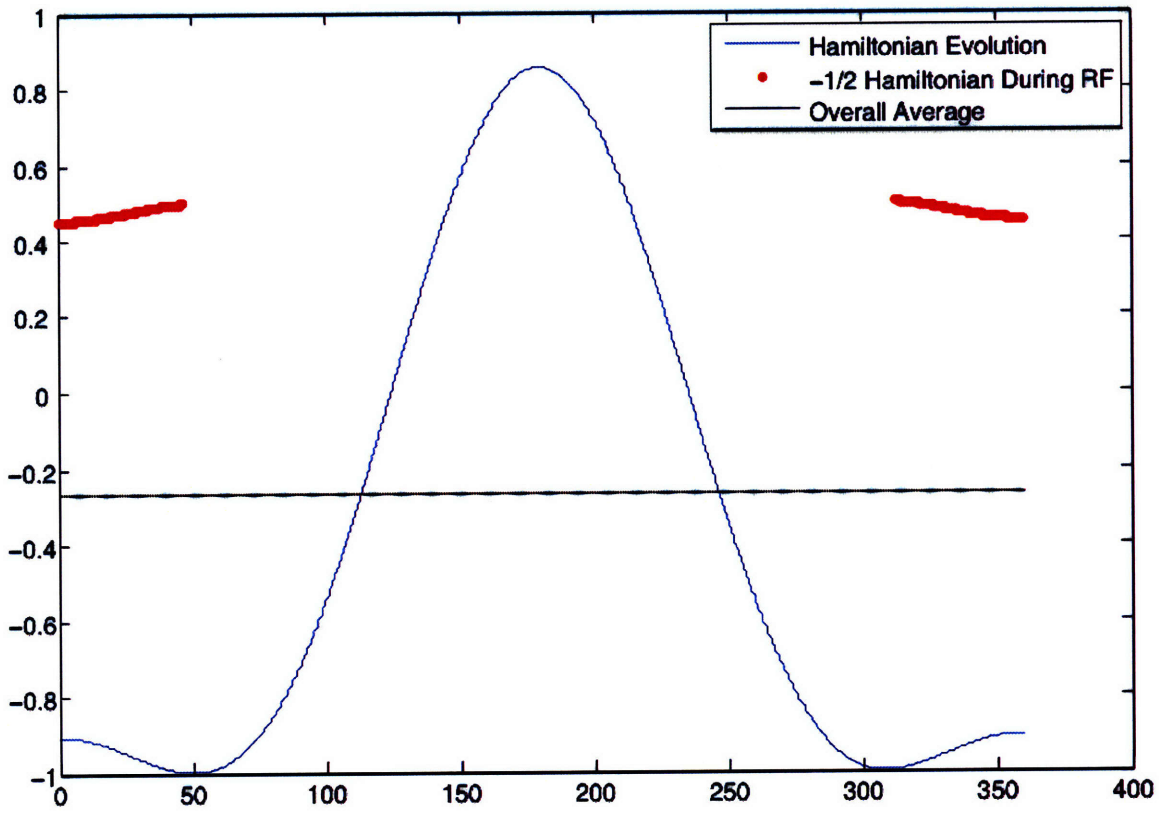

Figure 5-2: Evolution of on-chain Hamiltonian ($\theta = 10.3°$, $\theta_r = 31.1°$, pulse begins at $\psi = 312.7°$ and lasts $94.7°$)

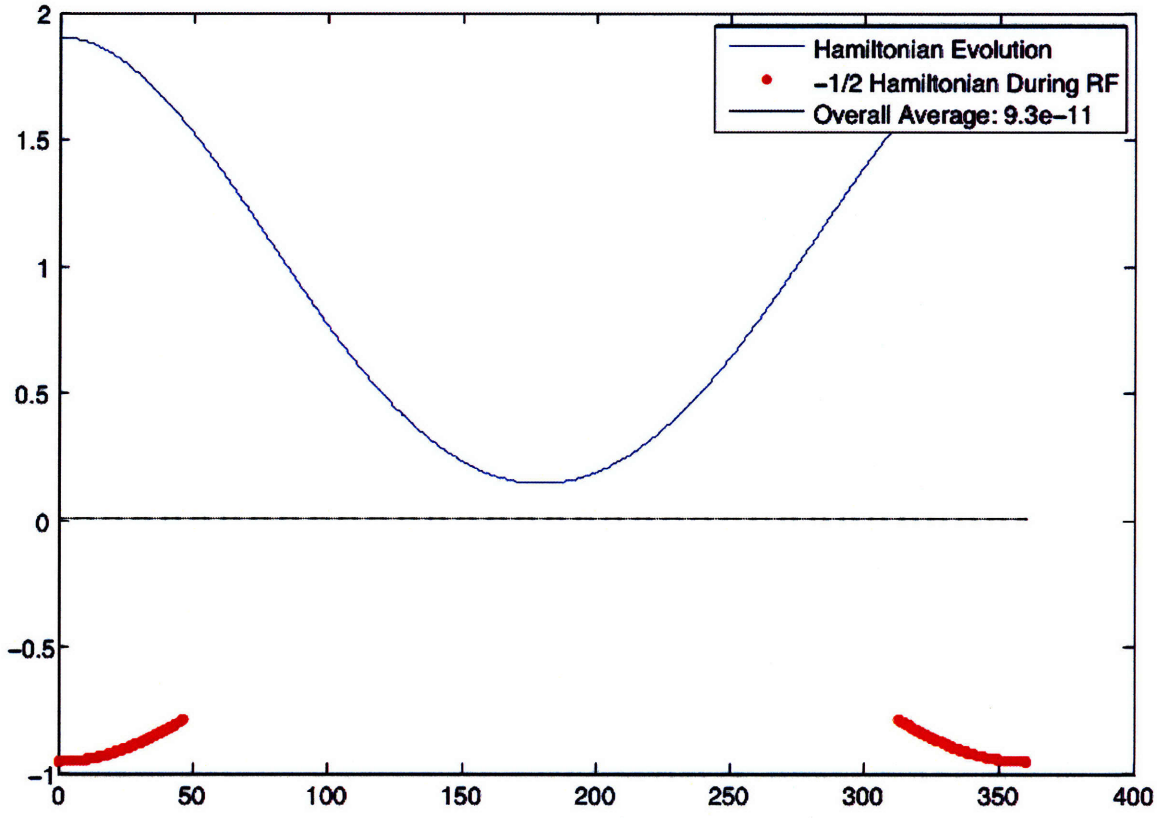

Figure 5-3: Evolution of off-chain Hamiltonian ($\theta = 10.3°$, $\theta_r = 31.1°$, pulse begins at $\psi = 312.7°$ and lasts $94.7°$)

Chapter 6

Conclusion

Thus, in this thesis, I have explored the dynamics of multiple quantum coherences, both aligned with magnetic field, as well as aligned with the magic angle. The field-aligned system's coherences oscillate as expected, but indicate that the spin chains present are likely to be longer than the 10–11 previously observed [4].

The dynamics of the magic angle-oriented system represent an intriguing area for further development. It is unexpected that no significant evolution had been observed by that far into a period of its primary dipolar coupling. More experiments will be needed to confirm and explore this effect.

Most interesting are the new possibilities created by the technique for selecting wanted couplings. This technique allows us in principle to create a very good analog of a 1D spin chain, allowing much of the theoretical work done on this system to be realized in experiments. Even more intriguingly, this technique is not limited to spin chains, or even to quasi-1D systems. It can be used to selectively cancel couplings in a wide array of systems, improving our ability to simulate complex quantum spin dynamics.

So how can we move forward? The next step for the coupling technique is clear. First, we need to simulate its evolution under realistic conditions; that is, numerical integration of the Hamiltonian of a crystal on a realistic rotor system, to confirm that it really works as well as it seems to.

Next, we need to improve the search process. For one thing, `fmincon`'s strin-

gent requirement of reducing the undesired coupling by 9–10 orders of magnitude is unnecessary—3, perhaps even 2, ought to suffice for most matters, and might result in improved amplitudes for the desired couplings. Also, the use of `fmincon`, a derivative-based search algorithm, is vulnerable to local minima. It is possible that better solutions could be reached if we moved to a grid-based method, or some combination of the two. Furthermore, we should move to a more realistic model of FAp. The current "toy model" involving just on-chain couplings and the three most powerful off-chain couplings may or may not paint a realistic picture of the dynamics under such a system; moving to a more robust model would help us to be sure.

Finally, if the results of these theoretical explorations are positive, the technique should be explored experimentally. This will require the creation of benchmarks that allow us to verify that the technique is working; that is, that the chains are not interacting with each other.

Appendix A

MQC Simulations

This appendix contains listings of the MATLAB scripts used to simulate the dynamics of spin chains at different angles.

A.1 spinshex.m

```
function meas=spins(spins, coords, m, t)
sx = [0 1; 1 0];
sy = [0 -i; i 0];
sz = [1 0; 0 -1];
si = [1 0; 0 1];
sp = sx + i*sy;
sm = sx - i*sy;

dnn = 1;
dnnn = dnn/8;

init = 0;
for j=0:spins-1
        init = init + tensor({si,j},sx, {si,spins-j-1});
end
```

```
H = 0;
for j=0:spins-2
        for jk=0:spins-2-j
                H=H+(3*cos(atan2(sqrt((coords{j+1}(1)
                        -coords{j+jk+2}(1))^2
                +(coords{j+1}(2)-coords{j+jk+2}(2))^2),
                        coords{j+1}(3)
                -coords{j+jk+2}(3)))^2 - 1)
                /sum((coords{j+1}-coords{j+jk+2}).^2)^(3/2)
                *(2*(tensor({si,j},sz,{si,jk},sz,{si,spins-2-j-jk}))
                -(tensor({si,j},sx,{si,jk},sx,{si,spins-2-j-jk})
                +tensor({si,j},sy,{si,jk},sy,{si,spins-2-j-jk})));
        end
end

s = expm(i*H*t)*init*expm(-i*H*t);

if m==1 %sigma z1
        meas = trace(tensor(sz,{si,spins-1})*s);
elseif m==2 %sum sigma z
        m0 = 0;
        for j=0:spins-1
                m0 = m0 + trace(tensor({si,j},sz,{si,spins-1-j})*s);
        end
        meas = m0;
elseif m==3 %nn zero-quantum
        m0 = 0;
        for j=0:spins-2
                m0 = m0 + trace(tensor({si,j},sp,sm,{si,spins-2-j})*s)
```

```
                + trace(tensor({si,j},sm,sp,{si,spins-2-j})*s);
        end
        meas = m0;
elseif m==4 %nn double-quantum
        m0 = 0;
        for j=0:spins-2
                m0 = m0 + trace(tensor({si,j},sp,sp,{si,spins-2-j})*s)
                + trace(tensor({si,j},sm,sm,{si,spins-2-j})*s);
        end
        meas = m0;
elseif m==5 %nn quadrupule-quantum
        m0 = 0;
        for j=0:spins-4
                m0 = m0
                + trace(tensor({si,j},sp,sp,sp,sp,{si,spins-4-j})*s)
                + trace(tensor({si,j},sm,sm,sm,sm,{si,spins-4-j})*s);
        end
        meas = m0;
elseif m==6 %sigma z2
        meas = trace(tensor(si,sz,{si,spins-2})*s);
elseif m==7 %sigma z3
        meas = trace(tensor({si,2},sz,{si,spins-3})*s);
elseif m==8 %sigma z4
        meas = trace(tensor({si,3},sz,{si,spins-4})*s);
elseif m==9 %sigma z5
        meas = trace(tensor({si,4},sz,{si,spins-5})*s);
elseif m==10 %sigmaxsigmay - sigmaysigmax
        m0 = 0;
        for j=0:spins-2
                m0 = m0
```

```
                + trace(tensor({si,j},sx,sy,{si,spins-2-j})*s)
                - trace(tensor({si,j},sy,sx,{si,spins-2-j})*s);
        end
        meas = m0;
elseif m==11 %sum sigma x
        m0 = 0;
        for j=0:spins-1
                m0 = m0 + trace(tensor({si,j},sx,{si,spins-1-j})*s);
        end
        meas = m0;
end
```

A.2 runhex.m

```
x=[0:.01:pi];

numspins=5;
measurement=11;
allz1 = [];
allz2 = [];
allz3 = [];
range=0:1:90
for t=range
        t
        t = t*pi/180
        m = [1 0 0; 0 cos(t) sin(t); 0 -sin(t) cos(t)];
        % o o     ^
        %o    o    |
        % o o     |
        coords1 = {m*[-1;0;0],m*[-1/2;0;sqrt(3)/2],
```

```
        m*[-1/2;0;-sqrt(3)/2],m*[1/2;0;sqrt(3)/2],
        m*[1/2;0;-sqrt(3)/2],m*[1;0;0]};

%  o       ^
%o   o     |
%o   o     |
%  o       |
coords2 = {m*[0;0;-1],m*[sqrt(3)/2;0;-1/2],
        m*[-sqrt(3)/2;0;-1/2],m*[sqrt(3)/2;0;1/2],
        m*[-sqrt(3)/2;0;1/2],m*[0;0;1]};

%o
%o   o
%o   o
%o
coords3 = {m*[0;0;0], m*[0;0;1], m*[0;0;2],
        m*[0;0;3], m*[3;0;1], m*[3;0;2]};
y1=[];
y2=[];
y3=[];
for k=1:length(x)
        y1 = [y1 spinshex1(6,coords1,measurement,x(k))];
        y2 = [y2 spinshex1(6,coords2,measurement,x(k))];
        y3 = [y3 spinshex1(6,coords3,measurement,x(k))];
end

allz1 = [allz1; y1];
allz2 = [allz2; y2];
allz3 = [allz3; y3];
end
```

```
figure;
surf(x, range, real(allz1));
figure;
surf(x, range, real(allz2));
figure;
surf(x, range, real(allz3));
```

Appendix B

Coupling Cancellation Scripts

This appendix contains listings of the MATLAB scripts used to search for optimal rotation schemes to cancel couplings, and to simulate the dynamics of spin chains under these schemes.

B.1 Search Scripts

B.1.1 `spindipham.m`

```
% clarification on variables: "oldx" is the old coordinates of the
% second spin.
% "newx" is the new coordinates of the second spin. Just "x" is
% the vector of theta, thetar, the start of the pulse, and the end
% of the pulse, all in radians. the first spin stays at origin
% throughout.

function h=spindipham(theta, phi, thetar, alphat);

oldx = [cos(phi)*sin(theta); sin(phi)*sin(theta); cos(theta)];
negry = [cos(thetar), 0, -sin(thetar); 0, 1, 0; sin(thetar), 0,
                cos(thetar)];
```

```
ry = [cos(thetar), 0, sin(thetar); 0, 1, 0; -sin(thetar), 0,
                cos(thetar)];
h = [];

for k=1:1:length(alphat)
        rz = [cos(alphat(k)), -sin(alphat(k)), 0; sin(alphat(k)),
                cos(alphat(k)), 0; 0, 0, 1];
        newx = negry*rz*ry*oldx;

        h = [h (3*newx(3)^2 - 1)];
end
```

B.1.2 minimizeme.m

```
% note: negative, since we are minimizing

function h=minimizeme(x)

h = .5 * quad(@(alphat)spindipham(x(1),0,x(2),alphat),x(3),x(3)+x(4))
        - quad(@(alphat)spindipham(x(1),0,x(2),alphat),x(3)+x(4),x(3)
        + 2*pi);
```

B.1.3 offcenterconstraints.m

```
function [c, ceq]=offcenterconstraints(x)

c = [];
ceq = [-.5 * quad(@(alphat)spindipham(pi/2+x(1),0,x(2),alphat),x(3),
                x(3)+x(4))
        + quad(@(alphat)spindipham(pi/2+x(1),0,x(2),alphat),x(3)+x(4),
                x(3)+2*pi);
         -.5 * quad(@(alphat)spindipham(pi/2+x(1),2*pi/3,x(2),alphat),
```

```
            x(3),x(3)+x(4))
        + quad(@(alphat)spindipham(pi/2+x(1),2*pi/3,x(2),alphat)
            x(3)+x(4), x(3)+2*pi);
        -.5 * quad(@(alphat)spindipham(pi/2+x(1),4*pi/3,x(2),alphat),
            x(3),x(3)+x(4))
        + quad(@(alphat)spindipham(pi/2+x(1),4*pi/3,x(2),alphat),
            x(3)+x(4),x(3)+2*pi)];
```

B.1.4 plotx.m

```
if (x(3)+x(4)>2*pi)
        xrf0 = 0:.001:(x(3)+x(4)-2*pi);
        xrf1 = x(3):.001:2*pi;
        xnorf0 = (x(3)+x(4)-2*pi):.001:x(3);
        xnorf1 = [];
else
        xrf0 = [];
        xrf1 = x(3):.001:x(4);
        xnorf0 = 0:.001:x(3);
        xnorf1 = x(4):.001:2*pi;
end

yrf0 = spindipham(x(1)+pi/2,0*pi/3,x(2),xrf0);
yrf1 = spindipham(x(1)+pi/2,0*pi/3,x(2),xrf1);
ynorf0 = spindipham(x(1)+pi/2,0*pi/3,x(2),xnorf0);
ynorf1 = spindipham(x(1)+pi/2,0*pi/3,x(2),xnorf1);

plot([xrf0 xnorf0 xrf1 xnorf1]*180/pi,[yrf0 ynorf0 yrf1 ynorf1], 'b',
        [xrf0*180/pi xrf1*180/pi], [-.5*yrf0 -.5*yrf1], 'r.',
        0:.1:360, fval/(2*pi), 'k')
legend('Hamiltonian Evolution','-1/2 Hamiltonian During RF',
```

```
        'Overall Average: 9.3e-11')
```

B.1.5 Example Usage

To use this code, for example, one might invoke MATLAB's `fmincon` like follows:

```
>> x = fmincon(@minimizeme, [0;pi/6;3*pi/2;pi],[],[],[],[],[0;0;0;0],
        [2*pi;2*pi;2*pi;2*pi],@offcenterconstraints)
```

This tells it to minimize the function `minimizeme`, that is, preserve the on-chain coupling, with no linear constraints, while obeying the nonlinear constraints of `offcenterconstraints` (all off-chain couplings must integrate to 0), and to search from 0–2π for each variable, with $[0; \pi/6; 3 * \pi/2; \pi]$ as the initial values.

Bibliography

[1] E. R. ANDREW, A. BRADBURY, and R. G. EADES. Nuclear magnetic resonance spectra from a crystal rotated at high speed. *Nature*, 182(4650):1659–1659, 1958.

[2] E. R. ANDREW, A. BRADBURY, and R. G. EADES. Removal of dipolar broadening of nuclear magnetic resonance spectra of solids by specimen rotation. *Nature*, 183(4678):1802–1803, 1959.

[3] D. Barnaal and I. J. Lowe. Effects of rotating magnetic fields on free-induction decay shapes. *Phys. Rev. Lett.*, 11(6):258–260, Sep 1963.

[4] Paola Cappellaro. *Quantum Information Processing in Multi-Spin Systems.* PhD dissertation, MIT, Department of Nuclear Science and Engineering, June 2006.

[5] Paola Cappellaro, Chandrasekhar Ramanathan, and David G. Cory. Dynamics and control of a quasi-1d spin system, 2007.

[6] Paola Cappellaro, Chandrasekhar Ramanathan, and David G. Cory. Simulations of information transport in spin chains, 2007.

[7] G. Cho and J. P. Yesinowski. Multiple-quantum NMR dynamics in the quasi-one-dimensional distribution of protons in hydroxyapatite. *Chemical Physics Letters*, 205:1–5, April 1993.

[8] G. Cho and J.P. Yesinowski. 1h and19f multiple-quantum nmr dynamics in quasi-one-dimensional spin clusters in apatites. *Journal of Physical Chemistry*, 100(39):15716–15725, 1996.

[9] I. L. Chuang, L. M. K. Vandersypen, X. Zhou, D. W. Leung, and S. Lloyd. Experimental realization of a quantum algorithm. *Nature*, 393:143–146, May 1998.

[10] Randall S. Dumont, Paul Hazendonk, and Alex Bain. Dual lanczos simulation of dynamic nuclear magnetic resonance spectra for systems with many spins or exchange sites. *The Journal of Chemical Physics*, 113(8):3270–3281, 2000.

[11] M. Engelsberg, I. J. Lowe, and J. L. Carolan. Nuclear-Magnetic-Resonance Line Shape of a Linear Chain of Spins. *Physical Review B*, 7:924–929, February 1973.

[12] Walter I. Goldburg and Moses Lee. Nuclear magnetic resonance line narrowing by a rotating rf field. *Phys. Rev. Lett.*, 11(6):255–258, Sep 1963.

[13] David J. Griffiths. *Introduction to Quantum Mechanics.* Pearson-Prentice Hall, Upper Saddle River, New Jersey, 2nd edition, 2005.

[14] Horst Kessemeier and Won-Kyu Rhim. Nmr line narrowing by means of rotary spin echoes. *Phys. Rev. B*, 5(3):761–768, Feb 1972.

[15] B. W. Lovett. Global optical control of a quantum spin chain. *New Journal of Physics*, 8:69–+, May 2006.

[16] I. J. Lowe. Free induction decays of rotating solids. *Phys. Rev. Lett.*, 2(7):285–287, Apr 1959.

[17] Michael Mehring. *Principles of High Resolution NMR in Solids.* Springer-Verlag, Heidelberg, Germany, 2nd edition, 1983.

[18] W-K. Rhim, A. Pines, and J. S. Waugh. Time-reversal experiments in dipolar-coupled spin systems. *Phys. Rev. B*, 3(3):684–696, Feb 1971.

[19] Won-Kyu Rhim and Horst Kessemeier. Transverse-magnetization recovery in the rotating frame. *Phys. Rev. B*, 3(11):3655–3661, Jun 1971.

[20] Charles P. Slichter. *Principles of Magnetic Resonance.* Springer Series in Solid-State Sciences 1. Springer-Verlag, Heidelberg, Germany, 3rd edition, 1992.